Experimental measurements of the residual solidification duration of a supercooled sodium acetate trihydrate

Noé Beaupere, Ulrich Soupremanien, Laurent Zalewski

Version of Record: https://www.sciencedirect.com/science/article/pii/S1290072920309972
Manuscript_d5c45d0bea9d050ae084500ff8a7d236

Experimental measurements of the residual solidification duration of a supercooled sodium acetate trihydrate

N. BEAUPERE [a, b]*, U. SOUPREMANIEN [a], L. ZALEWSKI [b]

[a] Université Grenoble Alpes, CEA Grenoble, CEA/LITEN/DTNM/SA3D/LMCM, 38000 Grenoble, France,

[b] Université d'Artois, EA 4515, Laboratoire de Génie Civil et géo-Environnement (LGCgE), F-62400 Béthune, France

Abstract

Phase change materials, such as sodium acetate trihydrate, are efficient materials for Latent Heat Thermal Energy Storage (LHTES) according to their interesting thermal properties (high latent heat and specific heat). Their main drawback is a large degree of supercooling, up to 90 K for sodium acetate trihydrate, where the material may remain liquid below its melting point. However, heat could be released if the solidification could be triggered. For a better understanding of how heat is discharged after an initial cooling by external water flow and a solidification induction by seeding, the temperature was experimentally recorded to measure the residual solidification plateau duration. This experiment was repeated for different nucleation temperatures and fit well with the theoretical predictions. An increase of 90% in the solidification duration was observed when the supercooling degree dropped from 35 to 8 K. Thanks to an original experimental bench, this temperature record has been compared with a fully new method allowing the measurements of the material's opacification throughout the solidification process. Finally, two different opacification behaviors were observed for supercooling degrees below and above 20 K.

Nomenclature

Symbol	Unit	Name
C_P	J.kg^{-1}.K^{-1}	Specific heat capacity
h	W.m^{-2}.K^{-1}	Heat transfer coefficient
L	J.kg^{-1}	Latent heat
m	kg	Mass
P	W	Heat transfer rate
SF	%	Solid fraction consumed for recalescence
R	K.s^{-1}	Cooling rate
t	s	Time
T	K	Temperature
T_m	K	Melting temperature
T_n	K	Nucleation temperature
w	-	Mass fraction
Δt	s	Residual solidification duration
ΔT	K	Supercooling degree
σ		Standard deviation
X_S		Related to solid
X_L		Related to liquid
X_{loss}		Related to thermal loss
X_{exp}		Related to experimental data
X_{rec}		Related to recalescence
X_{SA}		Related to sodium acetate
X_{total}		Related to a total quantity

X_{th}		Related to theory
X_{∞}		Related to the external environment, far from the tube
X_{PCM}		Related to the phase change material

1. Introduction

Building is the sector where energy consumption's growth is the most important since 1973, mainly due to HVAC (Heating, Ventilation and Air Conditioning) and DHW (Domestic Hot Water) systems development [1]. This heat demand can be reduced by a better building's thermal insulation and improved thermal management, as it should be more and more dependent on renewable energies [2].

However, renewable energies are not generally available at the time they are needed. For such conditions, thermal energy storage (TES) can be used to reduce this temporal mismatch, and phase change materials (PCM) may constitute a very interesting solution as a large quantity of heat could be stored through their phase change [3]. Salt hydrates are some of the most interesting PCMs, with an appropriate melting point (between 270 and 390 K), high latent heat capacity (100-350 $J.g^{-1}$) [4]. The solid material also presents a density of approximately 1.7 and the specific heat capacity around 1.65 $J.g^{-1}.K^{-1}$ [5], which may ensure good latent heat storage.

The PCM generally presents a "passive" solidification as the material turns into solid when the temperature drops below the liquidus temperature. However, salt hydrates may remain liquid several tens of degrees below the melting point before the solidification occurs. This phenomenon is called supercooling and is generally avoided in PCM's applications because a very low temperature has to be reached. This removal of supercooling is favored by the use of nucleating agents as shown by a previous study [5]. Considered as a drawback, it may be turned into a benefit if a reliable way of triggering solidification is developed [5], as the heat would be stored in a supercooled liquid, with no need for insulation, and released on demand. A specific salt hydrate, sodium acetate trihydrate (SAT, melting point of 331 K) was selected for this study. The seeding technique was demonstrated by Sandnes [6] to be efficient, reproducible, easy-to-make. Therefore, this technique was used to trigger the solidification in this study. Recently, some applications were developed where a supercooled sodium acetate trihydrate was solidified by seeding, for solar thermal storage [7] or building energy storage [8].

For the development of such devices, the duration of heat release needs to be understood, predicted and controlled. This duration corresponds to the residual solidification until the heat has been fully released. The solidification behavior of a PCM considering supercooling has been calculated by Uzan et al [9] and more recently by Soni et al [10]. However, the solidification duration was not evaluated by these authors. Therefore, a methodology, inspired by the work of Yang et al. [11] performed on a Cu-Ni alloy, was developed for this study. For this purpose, an experimental bench has been designed to measure the residual solidification durations and compare them with this theoretical approach. Besides, different temperature ranges have been explored (to be representative of the different thermal environments) regarding potential applications. In the first part of the study, the analysis was performed using an in-situ thermocouple to determine locally the heat release duration and compare the results to existing theories. However, for dynamic techniques of solidification triggering [5] as electrical discharge or sonication, the thermocouple may act as support for nucleation and it needs to be avoided to better understand the crystallization behavior.

An original technique using a laser has been developed to follow the opacification of the material throughout solidification. This method was already used by some authors, as Qiu et al. [12], who

presented the laser transmittance as an effective method for solidification tracking in salt hydrates. However, the method was improved in this study that aims at identifying a possible correlation between heat release duration at melting temperature and laser signal evolution.

In addition, the influence of supercooling degree on opacification does not seem to have been studied, which also motivated this study. Moreover, the material needs to be maintained in a supercooled state before nucleation is triggered, as spontaneous solidification and phase dissociation need to be avoided. This is achieved by the addition of water, according to the extra water principle introduced by Furbo [13]. The concentration of water after addition, usually necessary for the comprehension of material data, can be simply obtained from a model proposed by Desgrosseilliers et al [14].

2. Materials and methods

2.1. Preparation of the material

The material selected is sodium acetate trihydrate ($CH_3COONa.3H_2O$), purchased from Sigma-Aldrich (BioXtra, 99 % purity). The thermal properties of the raw material (60.3 wt% of sodium acetate) were measured by DSC (Differential Scanning Calorimetry). The melting point was found to be 331 K and the solidification was about 243 K, in good accordance with the previous results of Wada et al [15]. Moreover, the latent heat capacity was found to be approximately 250 $J.g^{-1}$, close to the values of Araki et al [16].

As water is expected to increase the stability of the supercooling [13], 2.2 g of deionized water has been added to the PCM. This addition of water ensures good aging stability as presented by Kong *et al.* [17] and decrease the freezing point, ensuring supercooling maintain. Besides, it did not reduce too much the material latent heat capacity, which remains about 200 $J.g^{-1}$ for a 54 wt% of sodium acetate sample[16]. In order to avoid future water evaporation during the repeated heating, leading to the segregation of anhydrous salt, 5 mL of silicon oil (VWR, Silicon oil 100 cSt, $(C_2H_6OSi)_n$) covers the upper side of the supercooled phase change material.

2.2. Experimental setup description

2.2.1 Test section description

A 20 mL quartz tube (Verrerie Villeurbanaise) was filled with 12.9 g of the liquid SAT+water mixture. The test section is a 16 mm * 100 mm (diameter * height) tube, with a thickness of 1.5 mm, described in Figure 1 (a). It is completed by a flange to ensure a repeatable positioning by a home-made sample holder, whose 3D view is depicted in Figure 1 (b).

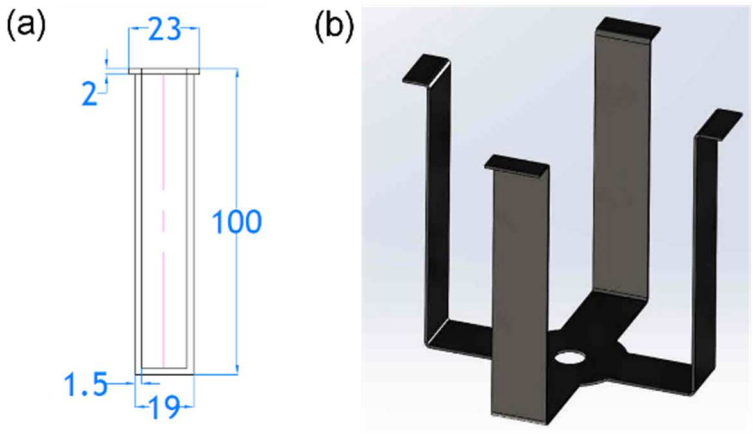

Figure 1 (a) Test section with dimensions and (b) sample holder

2.2.2. Melting of the SAT+water inside a reservoir put on a hot plate

The first step consisted in the immersion of the tube containing solid material in hot water, at a temperature of about 360 K, for a dozen minutes in order to fully melt the sample. A temperature of at least 20 K higher than the melting point should be reached in the tube to provide a stable supercooling state during cooling, as expected by Dannemand et al. [18].

2.2.3. Introduction of the tube into the thermally regulated tank.

Then, the tube was transferred to a PMMA (Poly-methyl methacrylate) tank (SinapTec) where the water temperature was set at 293 K, controlled by a chiller (Huber, Unichiller 012w). The sample was cooled down from 360 K, and the temperature was controlled by an in-situ K-type thermocouple positioned at the tube center. This thermocouple will serve for comparison with the theory. Then, to ensure the reliability of the laser signal opacification as an alternative method, the solidification duration measured by laser and thermocouple will be compared. When the material reached the desired temperature, it was solidified by seeding. Seeding corresponds to the introduction of a small crystal, whose mass approximates 2 mg. A representation of the experimental bench is given in Figure 2

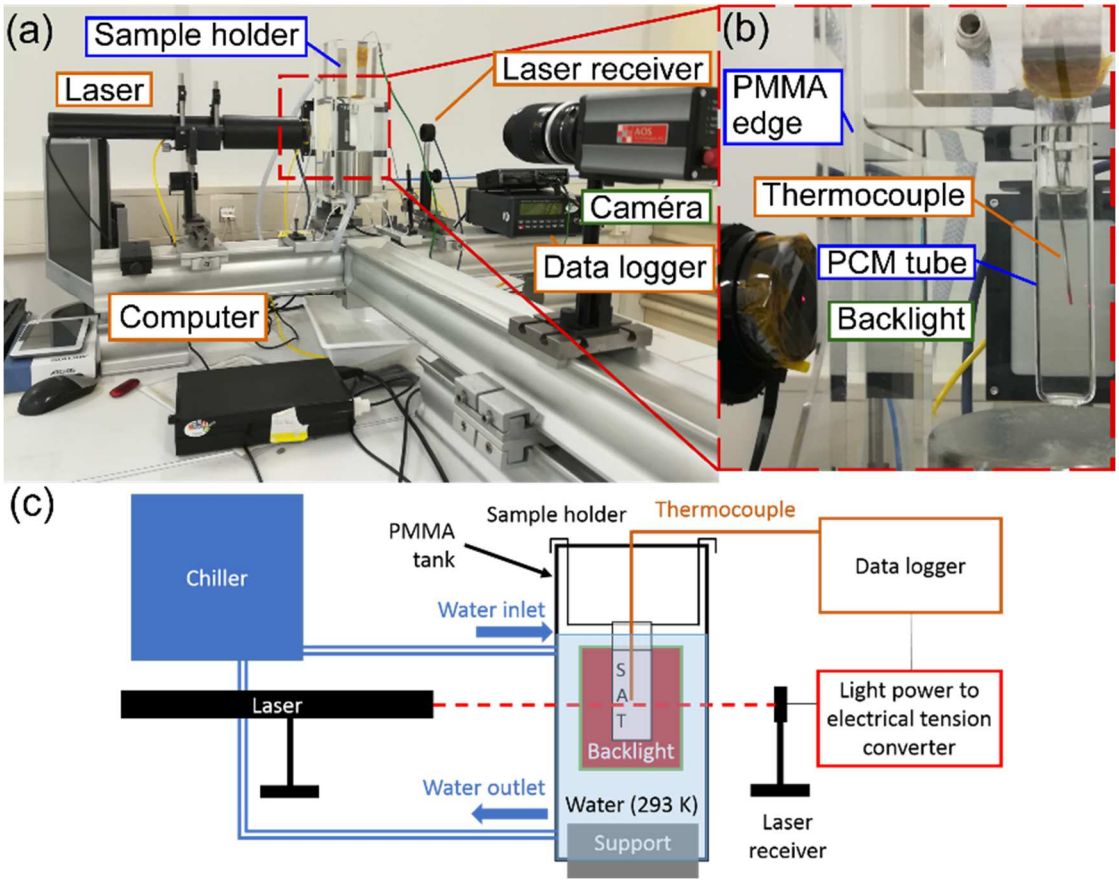

Figure 2 Experimental bench apparatus and (a) photo (b) tube containing the PCM in a bigger size and (c) front view

2.2.4 Measurement procedure

Once the crystallization was initiated in the tube, the solidification process was followed using a HeNe laser (Merles Griot, 05 LHR 171) with a wavelength of 633 nm. This value was chosen after a spectrophotometer analysis had been performed on a 10 mm deep sample, which showed a maximal specular transmittance plateau of 90 % (± 0.01 %) in the liquid phase and 0.08 % (± 0.01 %) in the solid phase between 500 and 700 nm.

By measuring the light power with a laser receiver (Newport, 818-SL) at any time, a full opacification of the material can be observed at the end of the solidification event. Indeed, the laser power passing through the liquid phase was about 500 µW (20,000 mV) and around 0.5 µW (20 mV) for the solid phase (far above the noise value, which was in the range of 0.01 µW). Data (temperature and laser signal) were recorded using an analogic data logger (Graphtec, Midi LOGGER GL220). This opacification measurement was compared with: 1) temperature evolution which used the K-type thermocouple immersed in the PCM and 2) video treatments from a high-speed camera (AOS Technologies, S-motion camera) with a backlight for increasing the contrast.

2.2.5 Water concentration determination using thermogravimetric analysis (TGA)

The water concentration in the PCM has to be determined as it is a critical value that drives the thermal properties of the water-sodium acetate, used later in this study for theoretical solidification duration calculation. TGA (Netzsch, Pegasus 449 F1) analysis was performed in order to measure the mass fraction of sodium acetate. About 50 mg of the sample was withdrawn from the middle height of the tube. Actually, this position was representative of the thermocouple and the laser ones, and its value would represent the local properties of the material. This sample was then heated up to 473 K, a temperature above the evaporation temperature of the water, allowing for the determination of a fully dry sample. A heating rate at 1 $K.min^{-1}$ was chosen for this characterization. Moreover, the sample was first kept at 303 K for 60 minutes, to ensure a constant value for the starting temperature. A second plateau was present at the maximal temperature to also ensure its stabilization. Indeed the stabilization of the temperature can be seen in Figure 3.

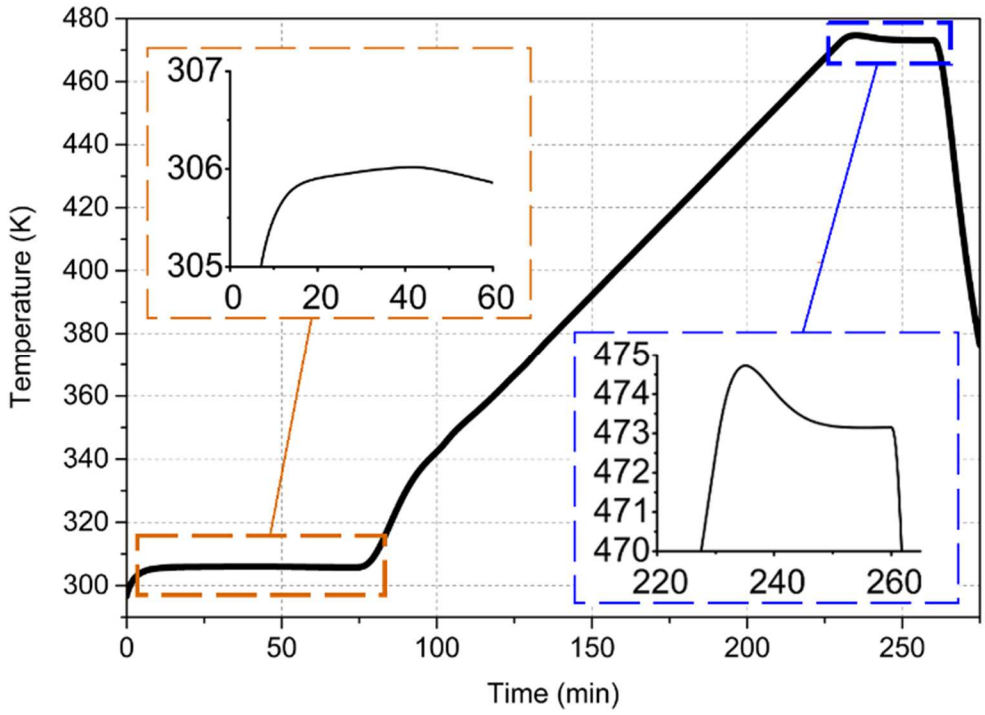

Figure 3 Temperature variation over time for TGA experiment

The water evaporation usually starts at 373 K and reaches a maximum of evaporation rate around 398 K [19]. Thus, the maximum temperature of 473 K was considered adapted for relevant observations. Then, the result of TGA is presented in Figure 4.

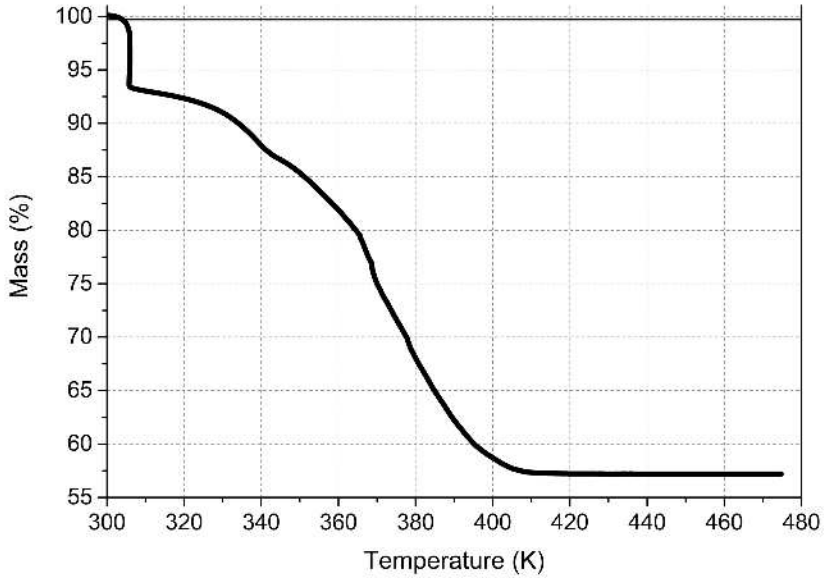

Figure 4 TGA result

The weight content is subjected to a first drop at 303 K, corresponding to the time when the temperature was maintained constant. Because of the use of dry air as injected gas, the water could easily evaporate from such a temperature as presented in Figure 3. A mass fraction (w_{SA}) of 0.5719 of sodium acetate was measured after this heating, corresponding to a fully dehydrated sample. However, this sodium acetate concentration may be changed throughout experiments, as a few volumes of pure sodium acetate trihydrate ($w_{SA} = 0.603$) was added every seeding. Nevertheless, this effect was considered negligible by the authors, as the crystal introduced for seeding add about 0.15 g of SAT in the volume, which represents a variation of 0.0012 in the mass fraction of the full sample.

3. Data reduction

3.1. Equations for material parameters calculation

For the comprehension of the thermal behavior of a material, it is necessary to determine its thermophysical properties. These properties have been experimentally measured by Araki et al. [16]. First, the specific heat capacity of the liquid has to be determined, because it defines the short-term energy storage, whose heat is released during the cooling of the supercooled sample. The evolutions of liquid specific heat capacity within a 303-353 K temperature range are presented in Eq. 1 and Eq. 2 for two concentrations. The error between the linear evolution and experimental points was said to be 5 %.

$$w_{SA} = 0.543 \qquad C_{P,L} = 1650 + 4.44 * T \qquad \text{Eq. 1}$$

$$w_{SA} = 0.603 \qquad C_{P,L} = 1560 + 4.27 * T \qquad \text{Eq. 2}$$

These equations were fitted by a first-order polynomial surface, given in Eq. 3. It allows for the calculation of the liquid heat capacity within a 330-350 K temperature range and a 0.543-0.603 sodium acetate mass fraction range. Moreover, the results were found to differ by less than 1 % in comparison to a second fit performed by Ma et al. [20].

$$C_{P,L} = 2460 + +5.97 * T + (-1500 - 2.833 * T) * w_{SA} \qquad \text{Eq. 3}$$

The solid specific heat is also important because it is representative of the heat needed to heat up the solidified material. This data was likewise measured by Araki et al. [16] at different temperatures for two ratios of sodium acetate. The Eq. 4 and Eq. 5 present a linear approximation of the evolution of solid specific heat for a 303-328 K temperature range, with an error less than 5 %.

$$w_{SA} = 0.543 \qquad C_{P,S} = 1360 + 2.58 * T \qquad \text{Eq. 4}$$

$$w_{SA} = 0.603 \qquad C_{P,S} = 811 + 4.06 * T \qquad \text{Eq. 5}$$

As before, a polynomial surface was used to fit the solid specific heat capacity, presented in Eq. 6. The approximation was considered valid for a 300-350 K temperature range, and a variation of w_{SA} from 0.543 to 0.603.

$$C_{P,S} = 6301 - 10.74 * T + (-9150 + 24.67 * T) * w_{SA} \qquad \text{Eq. 6}$$

The third material property needed for calculation is the latent heat capacity, which defines the efficiency of a latent heat storage device. This behavior was, as before, experimentally measured by Araki et al. [16] and approximated by a linear evolution, where the error remains below 5 % (Eq. 7). This equation was measured from w_{SA}= [0.45; 0.60].

$$L = -4{,}62 * 10^5 + 1{,}18 * 10^6 * w_{SA} \qquad \text{Eq. 7}$$

3.2. Equations for theoretical solidification duration calculation

Then, the supercooling degree is a key parameter for the determination of the duration of solidification, controlling its behavior. This corresponds to the difference between the melting temperature, assumed to be constant (331 K), and nucleation temperature. This supercooling degree is calculated using Eq. 8.

$$\Delta T = T_m - T_n \qquad \text{Eq. 8}$$

As the solidification may be influenced by the cooling parameters according to Bedecarrats et al [21], the cooling rate was introduced. This property gives a global overview of how the heat is released. This cooling rate *R* was calculated by Eq. 9 on the initial cooling slope before solidification was triggered by seeding.

$$R = (331 - 326)/\Delta t \qquad \text{Eq. 9}$$

As the cooling rate depends on temperatures of the PCM sample and water tank, it was estimated around the liquidus temperature (326-331 K), to be representative of residual solidification conditions as shown in Figure 5.

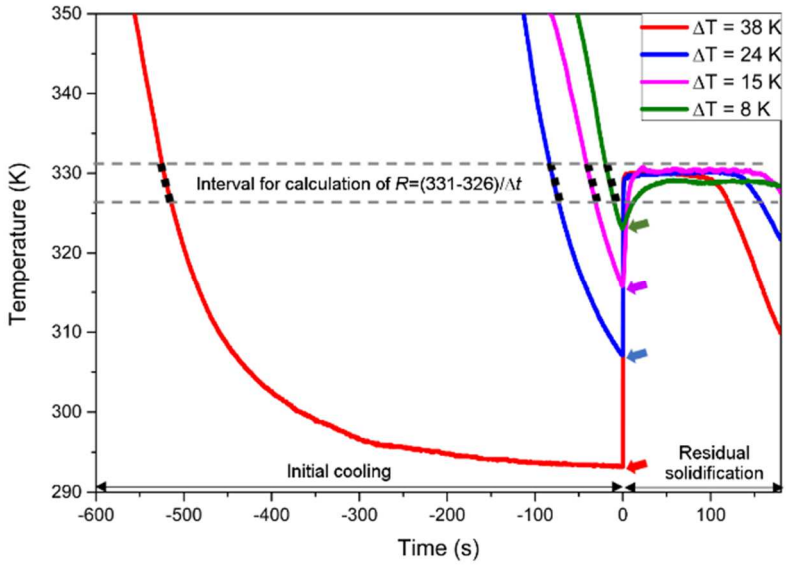

Figure 5 Presentation of the method for cooling rate calculation. The grey dashed line represents the temperature interval for residual solidification plateau. The black dotted lines symbolize the linear approximations for the cooling rate calculation (Eq. 9). The arrows indicate the seeding of supercooled samples.

Because the tube was cooled by water, the system was not considered adiabatic and a heat loss term was added as P_{loss}. This thermal loss was evaluated by the product of the mass of the sample, the specific heat and the cooling rate. Because a phase change from liquid to solid was evaluated, they were considered as extreme values to limit the results. A good correspondence was observed between the cooling rate of the full-liquid (before solidification) and the one of the full-solid (after solidification). Thus, the same cooling rate was considered, according to the Eq. 10.

$$P_{loss,i} = m * C_{P,i} * R \qquad \text{Eq. 10}$$

where i represents either the liquid or solid material. The thermal behavior during a phase change is involving a change of properties from liquid to solid. As nucleation started, a part of the material becomes solid and its latent heat is transferred to sensible heat to allow the material to return to the melting temperature. This process is known as recalescence. In order to investigate this change, the Eq. 11 investigates this change throughout an energy balance equation [9]. The final term of the equation represents the heat lost to the water tank by convection during rthe ecalescence step.

$$L * \frac{m_S}{m_{total}} = \frac{m_S}{m_{total}} C_{P,S}\Delta T + \left(1 - \frac{m_s}{m_{total}}\right) C_{P,L}\Delta T + \frac{P_{loss} * t}{m_{total}} \qquad \text{Eq. 11}$$

The part immediately solidified for recalescence is called SF. From Eq. 11, this solid fraction (SF) can be deduced [9]. Moreover, as this fraction corresponds to the formation of solid, the corresponding heat loss to water tank will be based on the time for recalescence. As said before, the letter i refer to either liquid or solid.

$$SF_i = \frac{m_S}{m_{total}} = \frac{C_{P,L}\Delta T + \frac{P_{loss,i} * t_{rec}}{m_S + m_L}}{L - C_{P,S}\Delta T + C_{P,L}\Delta T} \qquad \text{Eq. 12}$$

Then, the material reached a constant temperature slightly below the liquidus. This thermal plateau is related to an equivalence between the latent energy released and the heat extraction, as expressed in the Eq. 13.

$$\frac{dm}{dt} * L = \frac{(1 - SF)L}{m_{total}\Delta t} = hS(T_{PCM} - T_{\infty}) \quad \text{Eq. 13}$$

This heat extraction also equals the heat loss to the water tank by simple cooling of the material without any phase change, according to the Eq. 14.

$$hS(T_{PCM} - T_{\infty}) = m_{total}C_P R = m_{total}C_P \frac{dT}{dt} \quad \text{Eq. 14}$$

The solidification around the thermocouple ends when the temperature starts to decrease. The duration for the solidification of the residual liquid fraction, at a constant temperature, is calculated in Eq. 15 [11], being deduced from Eq. 13 and Eq. 14.

$$\Delta t_{th,i} = \frac{(1 - SF)L}{C_{P,i} * R} \quad \text{Eq. 15}$$

4. Results

4.1. Experimental measurements of the solidification plateau

Several experiments were carried out, separated in four ranges of nucleation temperatures. They were chosen as follow: a first range close to ambient temperature (293-298 K), then two intermediate ranges (304-310 K and 312-318 K) with a final range (321-325 K) close to the melting temperature of the material. Each range presents at least 10 experiments for repeatability. First, the solidification events were recorded by the camera, to give an overview of the different optical behaviors.

Then, to ensure the reliability of our results regarding the theory, experimental durations measured by a thermocouple were compared with theoretical ones. Then, a laser technique has been developed as an alternative method to not interact with the material (SAT). This external method may help for the limitation of heterogeneous solidification, possibly unwanted for solidification triggering comprehension experiments. Indeed, heterogeneous nucleation is favored by the presence of a metal surface as shown by Englmair et al [22] such as TC's one. Therefore, the solidification durations measured by TC and laser were compared in this study, to evaluate the results for the potential use of the laser method. Figure 6 presents snapshots from the camera, with temperatures corresponding to the different ranges, showing various behaviors. The snapshots were taken when an increase in temperature has been detected by the thermocouple (t = 0 s). This time also corresponds to the beginning of the material's opacification. As the laser beam is distant by less than 10 mm from the thermocouple and that the crystal is growing at a rate of 6 mm.s^{-1}, the solidifying front passes through the laser spot less than 2 seconds after the thermocouple. From the pictures, the repartition of the phases can be seen with (from bottom to top) liquid material turning into solid, water in excess, silicon oil, and air.

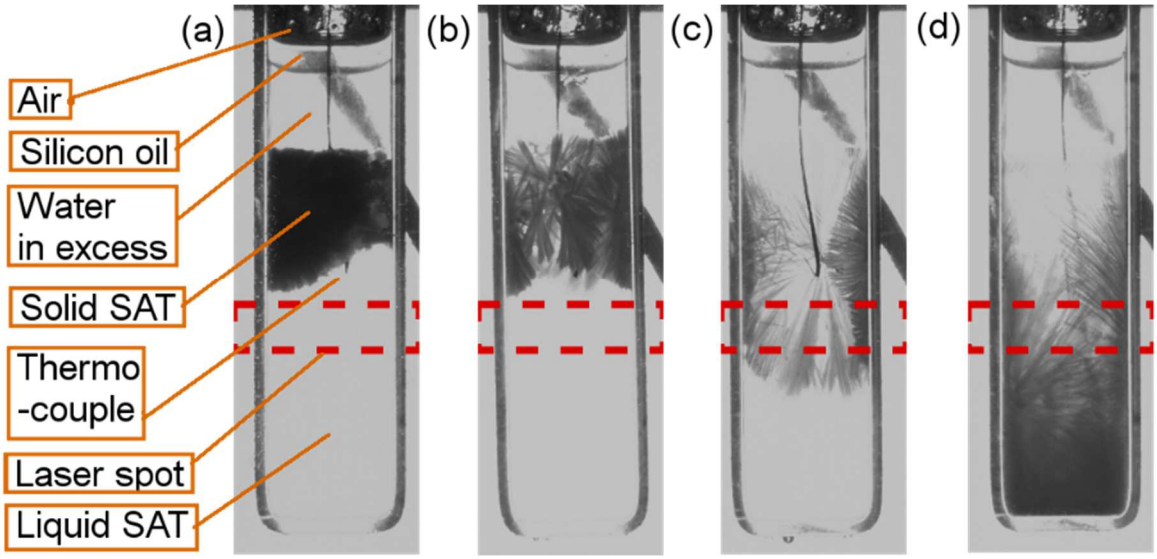

Figure 6 Solidification event for different supercooling degrees (a: ΔT = 37 K; b: ΔT = 24 K; c: ΔT = 15 K; d: ΔT = 8 K). The moment that snapshots are taken corresponds to the time that an increase of temperature was detected by the thermocouple

For a high supercooling degree (ΔT = 34 K, Figure 6 (a)), a large fraction of the material needs to be solidified to take back the temperature to melting point (331 K). This results in an important and rapid opacification, and the behavior is roughly the same for a sample supercooled by 23 K. The behavior becomes different as the nucleation temperature exceeds 310 K (ΔT < 20 K), as seen in Figure 6 (c) and (d). Because the phase change material is covered by silicon oil (as it shall limit water evaporation), the seed crystal is introduced at a higher temperature (6 K) , as it takes a few seconds to cross the surrounding oil. Indeed, the cooling rate was found to be about 0.5 $K.s^{-1}$ for the lowest supercooling experiment (ΔT = 8 K, Figure 6 (d)). For this experiment, the crystal was introduced around 331 K, where the solidification rate is so low that the crystal had time to reach the bottom of the tube before nucleation occurred. In addition, only a small fraction of the liquid was solidified for recalescence due to a low supercooling degree. Therefore, the material remained quite transparent, allowing us to follow the slow opacification of the material.

The evolutions of the power received from the laser and the temperature variations of the material during the solidification events were then recorded for numerous experiments, whose nucleation temperature were included in previously presented ranges. Four of them are presented in Figure 7, whose temperatures are representative of the different ranges, close to their mean values in terms of supercooling degrees, thermocouple and laser solidification durations. Figure 7 (a) and (b) present a sharp decrease of the laser signal to a minimum in the first seconds of opacification, before it re-increases. This phenomenon was not fully understood and may be due to optical effects (deflection of the laser path during the first stage of crystallization) rather than an opacification behavior of the material. Each laser signals were fitted to produce a monotonic trend by considering the second part of the signal only, allowing for comparison with other experiments. To do so, the laser signals obtained for low supercooling degrees (ΔT < 20 K) were first evaluated. A double exponential curve in the form of Eq. 16 was selected because it fits well the raw data (a coefficient of determination R^2 over 99.7 %) in the 50-300 s interval.

$$f(t) = A * \exp(B * t) + C * \exp(D * t) \qquad \text{Eq. 16}$$

This interval of time was chosen because it corresponds to the region of a monotonic decrease in the highly supercooled experiments (ΔT > 20 K). This fitting methodology was then applied to all these experiments, with a correct matching (R^2 > 99 %) in the 50-300 s interval also.

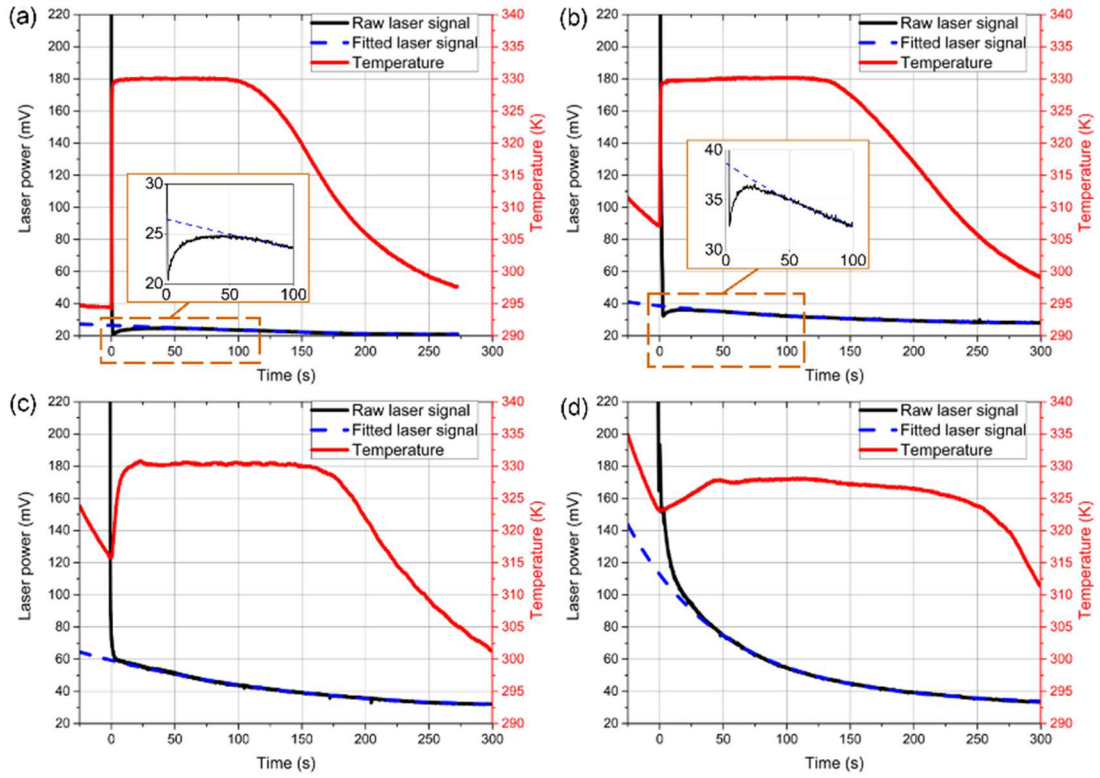

Figure 7 Temperature and received laser power over time for different supercooling degrees (a: ΔT = 37 K; b: ΔT = 24 K; c: ΔT = 15 K; d: ΔT = 8 K). Initial moment (time = 0 s) corresponds to the time that recalescence is detected by the thermocouple.

For a deeper analysis of Figure 7, the key parameters are reported in Table 1. The duration that has been considered for recalescence is the time needed to reach a variation of the temperature ($\Delta T/\Delta t$) close to zero while considering uncertainties of the measurement. Thus, a drop of the derivative of the temperature below a threshold of 0.05 $K.s^{-1}$ was found to be representative of the end of recalescence for the different experiments, as illustrated by Figure 8 (a). This recalescence part was not considered in solidification duration estimation, which only concerns residual solidification, as given in Eq. 15.

Table 1 Main parameters for laser and thermocouple signal evolution

ΔT (K)	37	24	15	8
T_n (K)	294	307	316	323
t_{rec} (s)	7,1	11,6	15,6	29,0
Maximal temperature reached (K)	330.3	330.4	331	328.3
Laser signal value after 300 s (mV)	20.9	28.1	32.1	33.4

Some trends are visible from these results. The duration for recalescence was multiplied by a factor of 4 when the supercooling degree moved from 37 K to 8 K. Therefore, the energy is released faster for a lower nucleation temperature. This can be related to a faster solidification rate at a deeper supercooling degree, as illustrated by Munakata et al. [23]. It is assumed that this faster solidification rate implies a faster heat extraction rate, as proposed by Dietz et al. [24].

The binary phase diagram from Green [25] shows that the liquidus temperature is between 330 K and 331 K for the trihydrate form. This temperature was reached in most of the experiments, but a lower temperature could be reached when the sample was supercooled by less than 10 K, as seen in Figure 7 (d).

Considering the laser signal, it is first important to notice a different behavior when the sample was supercooled by more than 20 K. The laser signal of those samples did not exceed 40 mV, or 30 mV when the supercooling degree was higher than 30 K, which made difficult the opacification analysis. On the contrary, the opacification for samples with a supercooling degree below 20 K presented in Figure 7 (c) and (d) started from a higher value, respectively 65 and 200 mV (1.6 and 5 µW) at a time of 0 s. This value of transmission is lower than in the fully liquid material (≈ 20,000 mV), mostly due to the opacification by solid parts located on the edges, as seen in Figure 6 (d). Then, the signal decreases softly to 33 mV, as the crystal grows to the center of the tube, reaching a minimum when the material is completely solid.

The reliability of these results was then evaluated regarding theory. The thermophysical properties were calculated from Eq. 1 through Eq. 7, adapted to a concentration of 57.19 wt% of sodium acetate, obtained from measurement with the TGA device. The theoretical solidification durations were determined using Eq. 15.

The experimental solidifications were considered achieved for the last moment that the derivative of temperature over time was equal to zero. However, the temperature was recorded every 100 ms with a precision of ± 0.1 K and was subjected to oscillations throughout the experiment, as shown in Figure 8 (black curve). They may hide a real decrease in temperature corresponding to the end of the solidification. To avoid such bias on the derivative calculation, the measured temperatures were approximated by a sliding average method.

The range of sliding average was selected to consider the totality of the isothermal plateau from all the experiments. Figure 8 presents the particular behavior of one of the samples nucleated at about 323 K (ΔT=8 K). This experiment presents a stabilization of the temperature around 215 s, which was considered as part of the residual solidification. Thus, the Figure 8 (b) focused on the different sliding average intervals at this moment, to select the largest range (for limitation of the oscillations from raw data) while being representative of the temperature stabilization. The dashed lines correspond to the times that solidification has been considered as completed (last moment that derivative is equal to zero) for the different sizes of sliding averages. Then, the temperature curves starts to have a linear tend, corresponding to the cooling of the solid material. Besides, the recalescence part, equal to 35 s for this experiment, was also depicted as the time that derivative becomes lower than 0.05 $K.s^{-1}$.

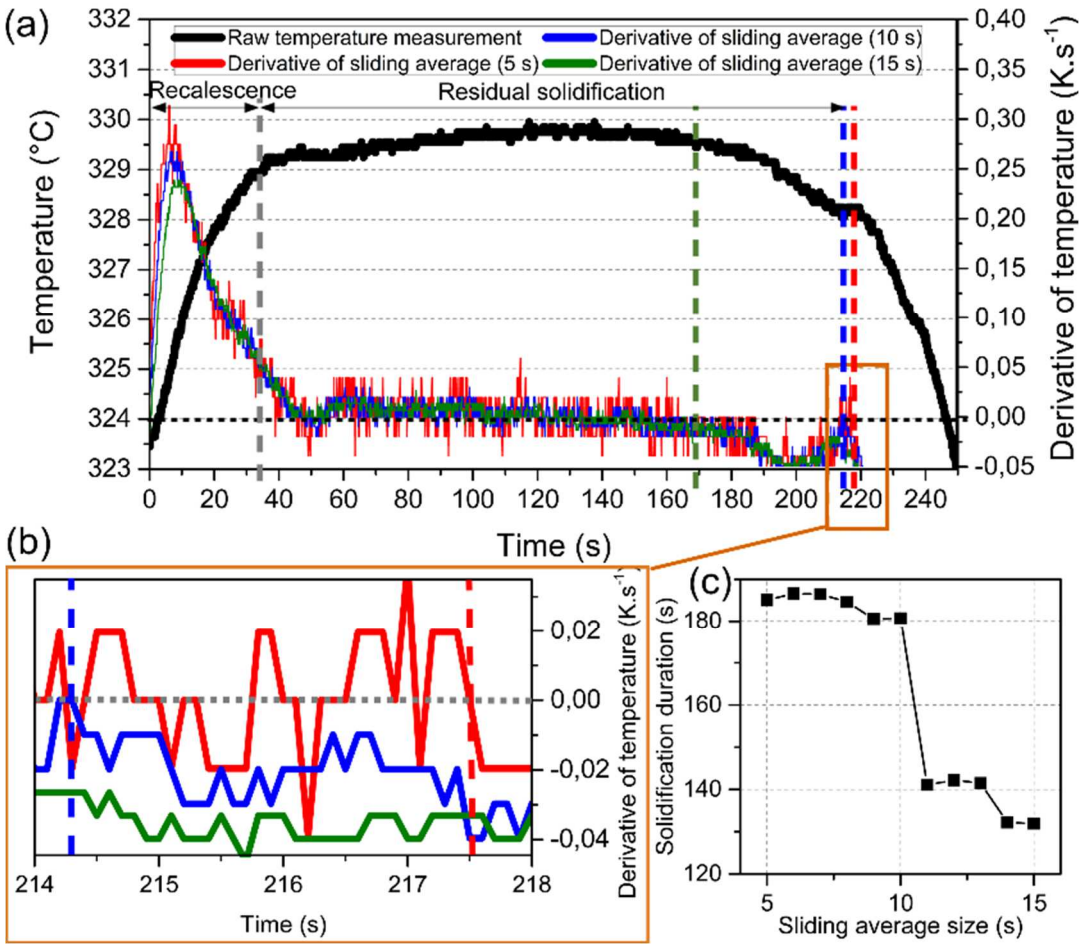

Figure 8 (a) Representation of the derivative values of sliding average for different intervals. The solidification duration for each interval (5 s; 10 s; 15 s) is indicated by the dashed lines and the end of recalescence by the grey dashed line; (b) Zoom on a [214; 218 s] time interval; (c) Evolution of solidification duration for different sliding average size. Recalescence duration was subtracted from the total one to obtain the plotted solidification duration.

From Figure 8, the averaging method with an interval of 9 s was found to be more representative of the total isothermal plateau for all the 45 realized experiments. Moreover, this value was considered stable as it was close to the neighboring ones (values for ± 1 s sliding average), which motivated the choice of this interval.

4.2. Comparison with theoretical calculations

The duration of solidification issued from a sliding average fit was finally compared with the theoretical calculations. The results presented in Table 2 are the mean values for the 4 ranges of temperature. Uncertainties on material properties (L, C_P) were 5 % of the value, as notified by Araki et al. [16].The uncertainties for the experimental parameters ($\Delta T, R, t_{rec}, \Delta t_{exp}$) were calculated to include 99.7 % of the values ($\pm 3\sigma$). Finally, the uncertainties for theoretical properties ($SF, \Delta t_{th}$) were determined by the error propagation method. Because the study involves phase change, the extreme theoretical durations were calculated by considering two values of thermal losses, either based on liquid or solid specific heats.

Table 2 Theoretical solidification duration parameters and comparison with the experimental duration

T_n (range, K)	293-298	304-310	312-318	321-325
ΔT (K)	35.6 ± 1.8	24.2 ± 1.8	15.4 ± 1.7	8.1 ± 1.0
L (*10^3 J.kg^{-1})	213 ± 11	213 ± 11	213 ± 11	213 ± 11
$C_{P,L}$ (*10^3 J.kg^{-1}.K^{-1})	2.89 ± 0.14	2.94 ± 0.15	2.98 ± 0.15	3.01 ± 0.15
$C_{P,S}$ (*10^3 J.kg^{-1}.K^{-1})	2.06 ± 0.10	2.10 ± 0.11	2.13 ± 0.11	2.16 ± 0.11
R (K.s^{-1})	-0.474 ± 0.016	-0.469 ± 0.019	-0.470 ± 0.022	-0.460 ± 0.020
$P_{loss,L}$ (W)	18.4 ± 1.1	18.3 ± 1.1	18.3 ± 1.1	17.9 ± 1.1
$P_{loss,S}$ (W)	13.2 ± 0.8	13.1 ± 0.8	13.1 ± 0.9	12.8 ± 0.8
t_{rec} (s)	7.1 ± 0.7	11.6 ± 4.6	15.6 ± 4.3	29.0 ± 5.6
SF_L (%)	47.6 ± 3.4	37.9 ± 3.0	30.1 ± 2.6	29.4 ± 1.9
SF_S (%)	46.4 ± 3.4	35.9 ± 2.9	27.3 ± 2.6	24.2 ± 1.8
$\Delta t_{th,L}$ (s)	77 ± 8	93 ± 9	104 ± 10	107 ± 10
$\Delta t_{th,S}$ (s)	110 ± 12	133 ± 13	151 ± 14	161 ± 14
$\Delta t_{exp}, thermocouple$ (s)	87 ± 9	118 ± 12	128 ± 12	148 ± 19

From Table 2, it is obvious that the solidification plateau is longer for higher temperature of nucleation, as less energy is lost by sensible heat during the cooling step. Besides, good consistency of the experimental heat release behavior was found regarding the theoretical calculations.

A general overview of the results performed in this study is given in Figure 9, with the duration of the solidification plateau over nucleation temperatures for all the experiments. The solidification durations were measured by the use of a sliding average, with an interval of 9 s. Because of the uncertainty on the choice of this interval, the error bars illustrate the values for an interval of $\pm$ 1 s (respectively 8 s for the upper one, and 10 s for the lower one). The theoretical data are represented by the black and red dashed curve, respectively for the liquid and solid phase.

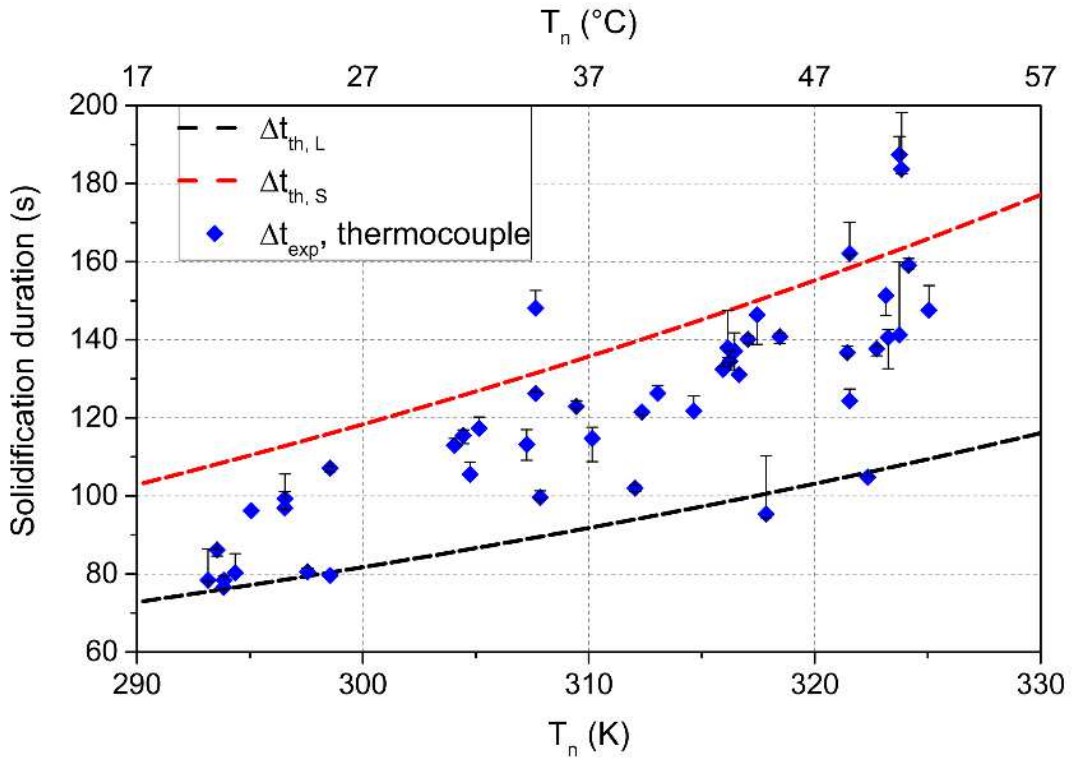

Figure 9 Plot of the solidification durations over triggering temperatures

From Figure 9, the experimental durations are shown to follow a linear trend for a crystallization temperature from 295 K to 320 K, close to theoretical calculation. Actually, about 85 % of the results are included in the solid-liquid range, which was considered acceptable for the consistency of our experimental results compare to the theory. The difference could be explained by the uncertainties of theoretical calculations, mainly dependent on the material properties.

4.3. Solidification durations estimated by laser signal analysis

As the thermocouple showed relevant results regarding theory, these data have been compared with a new method, using a laser, considered as non-intrusive. Indeed, the presence of a thermocouple would act as a substrate for heterogeneous nucleation, limiting the supercooling degree [5,22]. In our study, this substrate should not impact heat release duration as seeding was applied to trigger crystallization. This second method focuses on stabilization of the laser signal (fully opaque material) to indicate the end of the solidification plateau. Because this stabilization was difficult to evaluate due to its asymptotic behavior within time, an upper limit was set as a criterion, based on the percentage of the laser signal at 300 s, as expressed in Eq. 17

$$Upper\ limit\ (mV) = (laser\ value\ after\ 300\ s)(mV) * (1 + criterion) \qquad \text{Eq. 17}$$

Once the signal dropped below this limit, the material was considered fully solidified and the related time was set as solidification duration. Figure 10 presents the evolution of received laser signal over time, for the two extreme values of supercooling degrees (ΔT = 8 K and 34 K). The criterion's value is represented as a brown horizontal line in both graphs. In parallel, snapshots of the tube were taken at representative times, where the laser position is indicated by a rectangular dashed red line.

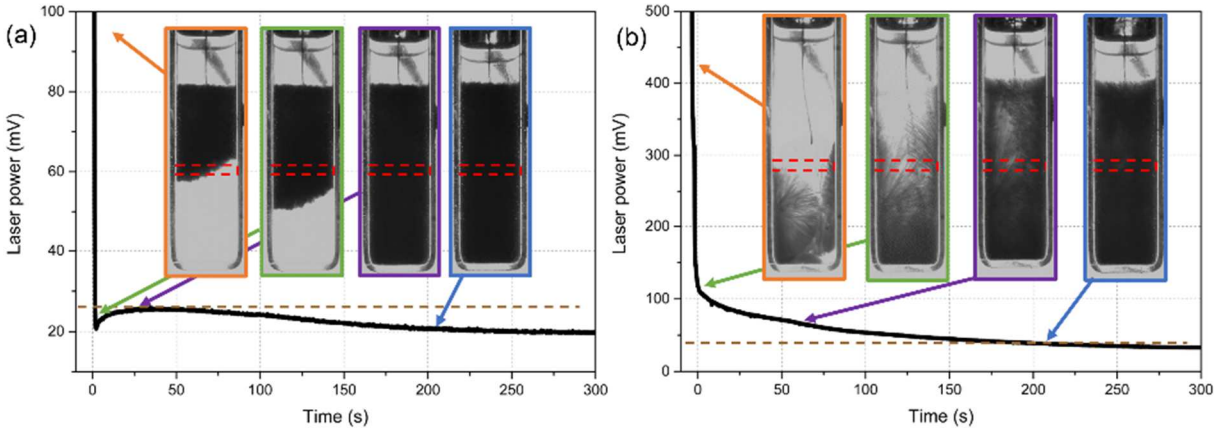

Figure 10 Opacification of the materials throughout solidification for a sample supercooled by (a) 34 K and (b) 8 K (the laser power scales are different for visibility). Brown dashed line represents the criterion value. Red dashed rectangle symbolize the laser path.

To set the criterion, the differences between the heat release duration measurement (using a thermocouple) that were considered to be consistent with the theory and the durations estimated using a laser method were evaluated. Because there was no possibility to dissociate recalescence duration with residual solidification for the laser study, it will also be included in the total solidification duration measured by the thermocouple. In order to minimize the difference between the solidification durations of the thermocouple and laser methods, a criterion of 25 % has been found. It has been decided to choose a confidence level of $\pm$ 20 % for the data calculated using this criterion to evaluate the difference between these two methods. The results comparing the two for a criterion of 25 % methods are presented in Figure 11 (a). Then, Figure 11 (b) gives an overview of the solidification durations evaluated by the over the supercooling degree.

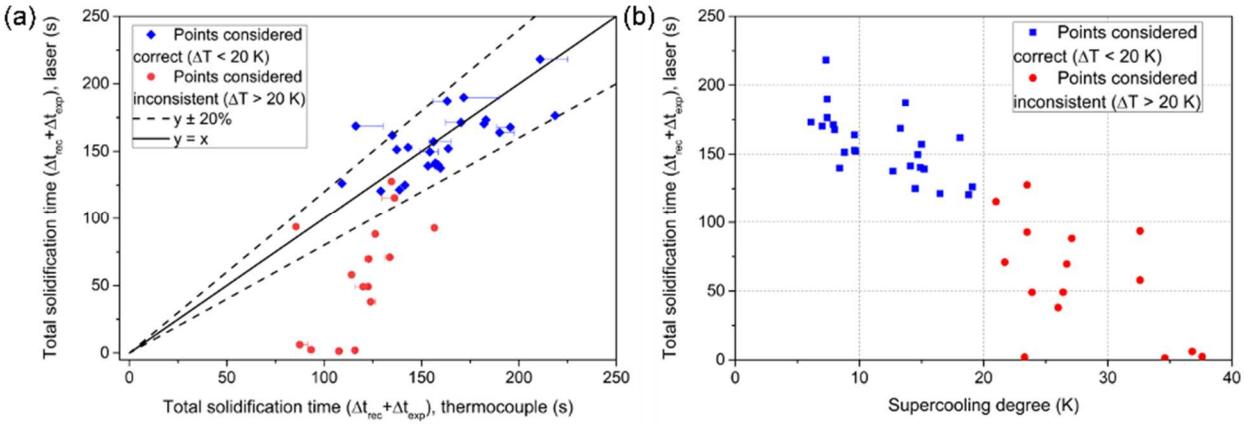

Figure 11 Laser duration over (a) thermocouple duration and (b) supercooling degree for a criterion of 25 %

From those figures, the evolution of the laser durations can be divided into two parts. The first part corresponds to a supercooling degree exceeding 20 K, whose laser's solidification duration is below 125 s, represented in red symbols in Figure 11. Their signals variations remained low, even after the fitted curve methodology was considered (see Figure 7). Indeed, as seen in Figure 6 (a), the material becomes immediately opaque after solidification started, leading to rapid obstruction of the laser beam. Thus, when the nucleation temperature is lower than 311 K (ΔT > 20 K), the material will present a particular behavior, not only dependent on material properties but also optical behavior. Less than half of the data for high supercooling (ΔT > 20 K) are visible on the graph, mostly because the fitted laser signal was lower than the criterion even before solidification occurs. So it may be concluded that the laser method could not be applied for such a deep supercooling degree. The second part, for supercooling degree below 20 K, corresponds to a solidification duration measured by laser above 125 s. For such values, the solidification duration measured by laser fitted well the one measured by the thermocouple, as 96 % of the experiments were within a $\pm$ 20 % interval. Besides, it has been noticed that this number varies negligibly when a bigger interval was chosen. According to Figure 7 (c) and (d), the laser signal had a continuous decrease over time for this range of temperature, so the solidification duration was considered correctly determined by the laser method. Therefore, better confidence may be placed in laser estimated heat release durations' values with a supercooling degree below 20 K, with a good consistency with the thermocouple method.

5. Conclusion

For the development of thermal energy long-term storage for building applications, the duration of residual solidification needed to be known to improve the development of an application. The durations were first determined from a thermocouple, by measuring the solidification thermal plateau. Different supercooling temperatures were tested, to be representative of different environments. Obviously, heat release is deeply influenced by the supercooling degree, as part of the heat stored could be lost by the initial cooling. This was illustrated by the recalescence step, consuming up to half of the latent heat stored for recalescence. The residual solidification and heat release duration was almost doubled when the supercooling degree was reduced from 34 to 8 K. After comparison with the theory, a good consistency was found as the differences may be due to uncertainties.

Then, this study intends to develop an external way of measuring the solidification duration by opacification. The laser signal passing through the phase change material was measured during

solidification. Afterward, a criterion was used to set the lower limit of the laser opacification, corresponding to the end of solidification. This home-made method seems to be efficient in measuring the solidification duration, specifically when the sample was nucleated above 310 K. This would help for the determination of heat release behavior when no contact is possible with the supercooled liquid.

However, a difference in behavior was observed depending on the nucleation temperature of the sample. It was noticed that above a threshold value (ΔT > 20 K), the material was already opaque so the laser signal immediately dropped below the limit set by the criterion. Besides, the signal decrease was not continuous but subjected to a singular behavior which does not allow a good consistency with theoretical data. So the results from such a deep supercooling degree were considered inconsistent.

This behavior was not observed for softly supercooled experiments (ΔT < 20 K), where a slower opacification of the material resulted in a continuous decrease of the laser signal. Thus, the method presented in this study was applicable, considering a material solidified as soon as the laser signal dropped below a set value. These different behaviors were also confirmed by cameras snapshots' analysis related to the solidification events.

6. References

[1] L. Pérez-Lombard, J. Ortiz, C. Pout, A review on buildings energy consumption information, Energy and Buildings. 40 (2008) 394–398. doi:10.1016/j.enbuild.2007.03.007.

[2] World Energy Outlook, IEA. (n.d.). https://www.iea.org/weo/ (accessed January 22, 2019).

[3] V.V. Rao, R. Parameshwaran, V.V. Ram, PCM-mortar based construction materials for energy efficient buildings: A review on research trends, Energy and Buildings. 158 (2018) 95–122. doi:10.1016/j.enbuild.2017.09.098.

[4] B. Zalba, J.M. Marín, L.F. Cabeza, H. Mehling, Review on thermal energy storage with phase change: materials, heat transfer analysis and applications, Applied Thermal Engineering. 23 (2003) 251–283. doi:10.1016/S1359-4311(02)00192-8.

[5] N. Beaupere, U. Soupremanien, L. Zalewski, Nucleation triggering methods in supercooled phase change materials (PCM), a review, Thermochimica Acta. 670 (2018) 184–201. doi:10.1016/j.tca.2018.10.009.

[6] B. Sandnes, J. Rekstad, Supercooling salt hydrates: Stored enthalpy as a function of temperature, Solar Energy. 80 (2006) 616–625. doi:10.1016/j.solener.2004.11.014.

[7] M. Dannemand, W. Kong, J. Fan, J.B. Johansen, S. Furbo, Laboratory Test of a Prototype Heat Storage Module Based on Stable Supercooling of Sodium Acetate Trihydrate, Energy Procedia. 70 (2015) 172–181. doi:10.1016/j.egypro.2015.02.113.

[8] L. Desgrosseilliers, Design and Evaluation of a Modular, Supercooling Phase Change Heat Storage Device for Indoor Heating, Thesis, 2017. https://DalSpace.library.dal.ca/handle/10222/73309 (accessed January 30, 2018).

[9] A.Y. Uzan, Y. Kozak, Y. Korin, I. Harary, H. Mehling, G. Ziskind, A novel multi-dimensional model for solidification process with supercooling, International Journal of Heat and Mass Transfer. 106 (2017) 91–102. doi:10.1016/j.ijheatmasstransfer.2016.10.046.

[10] V. Soni, A. Kumar, V.K. Jain, A novel solidification model considering undercooling effect for metal based low temperature latent thermal energy management, Journal of Energy Storage. 21 (2019) 528–542. doi:10.1016/j.est.2018.12.006.

[11] W. Yang, F. Liu, Z.F. Xu, B.P. Lu, G.C. Yang, Use of recalescence behavior analysis for the prediction of grain refinement in undercooled Cu–Ni alloy, J Mater Sci. 46 (2011) 3101–3107. doi:10.1007/s10853-010-5189-6.

[12] L. Qiu, L. Shi, Z. Liu, K. Xie, J. Wang, S. Zhang, Q. Song, L. Lu, Effect of power ultrasound on crystallization characteristics of magnesium ammonium phosphate, Ultrasonics Sonochemistry. 36 (2017) 123–128. doi:10.1016/j.ultsonch.2016.11.019.
[13] S. Furbo, Heat Storage with an Incongruently Melting Salt Hydrate as Storage Medium Based on the Extra Water Principle, in: Thermal Storage of Solar Energy, Springer, Dordrecht, 1981: pp. 135–145. doi:10.1007/978-94-009-8302-1_15.
[14] L. Desgrosseilliers, P. Allred, D. Groulx, M.A. White, Determination of enthalpy–temperature–composition relations in incongruent-melting phase change materials, Applied Thermal Engineering. 61 (2013) 193–197. doi:10.1016/j.applthermaleng.2013.07.019.
[15] T. Wada, F. Kimura, Y. Matsuo, Studies on Salt Hydrates for Latent Heat Storage. IV. Crystallization in the Binary System CH3CO2Na–H2O, BCSJ. 56 (1983) 3827–3829. doi:10.1246/bcsj.56.3827.
[16] N. Araki, M. Futamura, A. Makino, H. Shibata, Measurements of thermophysical properties of sodium acetate hydrate, Int J Thermophys. 16 (1995) 1455–1466. doi:10.1007/BF02083553.
[17] W. Kong, M. Dannemand, J.B. Johansen, J. Fan, J. Dragsted, G. Englmair, S. Furbo, Experimental investigations on heat content of supercooled sodium acetate trihydrate by a simple heat loss method, Solar Energy. 139 (2016) 249–257. doi:10.1016/j.solener.2016.09.045.
[18] M. Dannemand, J. Dragsted, J. Fan, J.B. Johansen, W. Kong, S. Furbo, Experimental investigations on prototype heat storage units utilizing stable supercooling of sodium acetate trihydrate mixtures, Applied Energy. 169 (2016) 72–80. doi:10.1016/j.apenergy.2016.02.038.
[19] R. Naumann, H. Emons, Results of thermal analysis for investigation of salt hydrates as latent heat-storage materials, Journal of Thermal Analysis and Calorimetry. 35 (1989) 1009–1031.
[20] Z. Ma, H. Bao, A.P. Roskilly, Study on solidification process of sodium acetate trihydrate for seasonal solar thermal energy storage, Solar Energy Materials and Solar Cells. 172 (2017) 99–107. doi:10.1016/j.solmat.2017.07.024.
[21] J.P. Bédécarrats, F. Strub, B. Falcon, J.P. Dumas, Phase-change thermal energy storage using spherical capsules: performance of a test plant, International Journal of Refrigeration. 19 (1996) 187–196. doi:10.1016/0140-7007(95)00080-1.
[22] G. Englmair, Y. Jiang, M. Dannemand, C. Moser, H. Schranzhofer, S. Furbo, J. Fan, Crystallization by local cooling of supercooled sodium acetate trihydrate composites for long-term heat storage, Energy and Buildings. 180 (2018) 159–171. doi:10.1016/j.enbuild.2018.09.035.
[23] T. Munakata, S. Nagata, Study on Solidification Process of Sodium Acetate Trihydrate from Supercooled State, Transactions of the Japan Society of Mechanical Engineers Series B. 74 (2008) 2365–2371. doi:10.1299/kikaib.74.2365.
[24] P.L. Dietz, J.S. Brukner, C.A. Hollingsworth, Linear Crystallization Velocities of Sodium Acetate in Supersaturated Solutions, J. Phys. Chem. 61 (1957) 944–948. doi:10.1021/j150553a023.
[25] W.F. Green, The “Melting-Point” of Hydrated Sodium Acetate: Solubility Curves, J. Phys. Chem. 12 (1907) 655–660. doi:10.1021/j150099a002.